



## Turbulence Modeling Comparative Analysis For Vertical Axis Wind Turbines

M. R. Rashed <sup>a,b</sup>, O. E. Abdellatif <sup>b</sup>, M. F. Abd Rabbo <sup>b</sup>, E. E. Khalil <sup>c</sup>, I. Shahin <sup>b</sup>

<sup>a</sup> Mechanical Engineering Dept., Faculty of Engineering-MTI University, Cairo, Egypt

<sup>b</sup> Mechanical Engineering Dept., Faculty of Engineering at Shoubra-Benha University, Cairo, Egypt

<sup>c</sup> Mechanical Power Engineering Dept., Faculty of Engineering-Cairo University, Giza, Egypt

### Abstract

The impact of turbulence model selection on the accuracy of CFD simulations of VAWTs is highly considered. In this paper 2D CFD simulations were carried out on a three-bladed H-Darrieus VAWT with NACA 0021 airfoil. Two turbulence models, two equations  $k-\epsilon$  Realizable and four equations Transition-SST, were selected to validate the power coefficient calculated from simulations with numerical and experimental data from the literature. The power coefficient calculated from the simulations performed by the  $k-\epsilon$  Realizable turbulence model was slightly underestimated, while Transition-SST turbulence model results were slightly overestimated. However, in terms of root mean square error of the power coefficient calculated from the simulations performed by the  $k-\epsilon$  Realizable turbulence model gives a value of 0.0503, while the Transition-SST model gives a value of 0.0655. Moreover, in terms of mean average percentage error of the power coefficient calculated from the simulations performed by the  $k-\epsilon$  Realizable turbulence model gives a value of 35.15%, while the Transition-SST model gives a value of 42.34%. Another validation with a two straight bladed numerical model with NACA 0018 airfoil was performed using 2D CFD simulations. Two equations  $k-\epsilon$  Realizable, two equations  $k-\omega$  SST and four equations Transition-SST were selected to conduct these simulations, the results showed that the  $k-\epsilon$  Realizable turbulence model was the best candidate among the other ones.

### 1 Introduction

Recently, utilization of renewable energy sources (e.g. wind, solar, geothermal, biomass, hydropower and ocean energies, etc.) have been hastened as a result of the growing fears of global warming, running out of fossil fuel resources, and firmer ecological rules in energy market [1]. Amongst renewable resources, wind energy jumped to be the frontrunner with almost 50% of total global installed renewable energy capacity (excluding hydroelectric energy) [2], and it has undergone an accelerated development worldwide. The total accumulative installed capacity of wind energy has been raised from 17 GW in 2000 to 540 GW in 2017 [3]. So far, wind turbines are the appropriate harvesters to capture and utilize such precious, valuable and sustainable energy. Wind turbines are mainly categorized into two categories based on the rotor shaft orientation relative to the airflow direction: horizontal axis wind turbines (HAWTs) and vertical axis wind turbines (VAWTs). HAWTs is the traditional shape extensively used for large-scale electric power generation as a result of several years of investigations and improvements [4]. However, during the last few years, VAWTs started to receive greater interest as wind energy harvesters for both off-shore applications, as well as the urban environment [5]. So far, the efficiency of VAWTs at this time is less than HAWTs [6]. Studies on VAWTs, regardless of their complicated aerodynamics, has been placed in the wakes of the

researches on HAWTs and from now attracted a relatively little attention during the last years [7]. The fundamental concept behind the generation of power via VAWTs is more complicated comparatively with HAWTs [8]. The intricacy could be mostly credited to the VAWT's fluctuating nature in terms of power generation which is caused by the great changes in the relative velocity and the angle of attack for each turbine one complete revolution [9]. Moreover, this could be associated with a number of complicated flow phenomena such as blade-wake interaction, dynamic stall, flow curvature effects, vortex shedding and Coriolis effect [10]. So as to enhance the aerodynamic performance of VAWTs, these complicated flow characteristics are required to be totally comprehended. Additionally, the influence of several operational and geometrical parameters on the aerodynamic performance of VAWTs is vital to be deeply described and assessed. The geometrical parameters consist of solidity, number of blades, blade pitch angle, airfoil shape and turbine shaft [11]. The operational parameters include Reynolds number, tip speed ratio and turbulence intensity [12].

Computational Fluid Dynamics (CFD) is one of the most numerical effective tools for such investigations and evaluations, accordingly, it has been extensively employed to study the aerodynamic performance of VAWTs [13]. Earlier CFD investigations involved attempts to explain the underlying physics causing the

unsteady power generation of the turbine [8] and to describe the aerodynamic performance of VAWTs under the effect of several operational and geometrical parameters [14]. Furthermore, a number of CFD investigations concentrated on increasing the aerodynamic performance of VAWTs through the blade pitch angle optimization [9], reducing the power loss [11], the using of flow control devices, ducts and guide vanes [15]. It is extensively known that the precision and reliability of CFD computations of VAWTs can be very delicate to the numerical settings. For instance, a number of earlier researches highlighted the major significance of azimuthal increment (which is expressed as the angle that a rotor turns each time step), computational domain dimensions [16] and convergence condition (described as the number of turbine cycles before achieving a statistically steady-state condition). The studies showed that the range of the azimuthal increment varies from  $0.03^\circ$  up to  $10^\circ$  [16]. However, in terms of convergence criterion, there was no exact consensus on how many turbine revolutions should be completed to reach convergence, some investigations [17] counted convergence from the 4th turbine revolution while other investigations considered this from 100th turbine revolution [16]. However, the aforementioned studies were case-specific studies and limited in scope, another later study focused on providing general guidelines and recommendations to serve future CFD studies on VAWTs. Rezaeiha et al. [16] concluded that in terms of domain size, the least upstream length from the center of turbine to the inlet of domain needs to be 15 times of the turbine diameter (15D), and the smallest downstream length from the center of turbine to the outlet of domain ranges between 10D up to 50D, however, a distance of 15D shows a quite reasonable results, and a domain with a width of 20D is required to reduce the impact of the blockage on the computations, while in terms of azimuthal increment, it was limited to be  $0.1^\circ$  for the low tip speed ratios, and  $0.5^\circ$  for high tip speed ratios, and finally in terms of convergence criterion, it was determined that the lowest possible number of turbine rotations to confirm that the computations have achieved a statistically steady-state condition ranges from 20 up to 30 turbine revolutions.

The accuracy and the efficiency of CFD solver required to be used to analyze the VAWTs simulations are strongly reliant on the choice of the turbulence model. The turbulence models presented are mostly based on averaging the transport quantities in the Navier—Stokes equations. In VAWTs, the transition of the flow from laminar to turbulent nearby the blade, the flow separation and the reattachment, and the laminar separation bubbles incidence on the airfoil surface are all very vital aspects that essential to be concerned about in the choice of the most suitable turbulence model [18]. Daróczy et al. [19] systematically studied and evaluated the experimentally determined characteristic curves with outcomes of several turbulence models utilizing CFD simulations with StarCCM+ and Fluent on H-Darrieus turbines, and deduced that k- $\epsilon$  Realizable and k- $\omega$  SST model are the best candidates in 2D simulation.

Lanzafame et al. [20] used k- $\omega$  SST and SST Transition model in 2D CFD computations to assess the performance of H-Darrieus turbines and determined that the SST Transition model is the best. Differently, Gosselin et al. [21] have examined SST Transition, k- $\omega$  SST with low Reynolds corrections and Spalart-Allmaras (with modified strain-based formulation) models, and determined that the k- $\omega$  SST model was the most suitable. Castelli et al. [22] found that k- $\omega$  SST model is the most suitable in 3D, while k- $\epsilon$  Realizable model is more accurate in 2D.

Obviously, there are still conflicting statements in the previous works involving the most applicable turbulence model for VAWTs CFD simulations.

## 2 Numerical Methodologies

### 2.1 Governing Equations

The numerical computations are completed with a two-dimensional unsteady turbulent flow system. Governing equations are:

Continuity equation:

$$\nabla \cdot (\rho \vec{V}) = 0 \quad (1)$$

Momentum equations:

X-momentum equation:

$$\begin{aligned} \frac{\partial(\rho u)}{\partial t} + \nabla \cdot (\rho u \vec{V}) \\ = -\frac{\partial p}{\partial x} + \frac{\partial \tau_{xx}}{\partial x} \\ + \frac{\partial \tau_{yx}}{\partial y} \end{aligned} \quad (2)$$

Y-momentum equation:

$$\begin{aligned} \frac{\partial(\rho v)}{\partial t} + \nabla \cdot (\rho v \vec{V}) \\ = -\frac{\partial p}{\partial y} + \frac{\partial \tau_{xy}}{\partial x} \\ + \frac{\partial \tau_{yy}}{\partial y} \end{aligned} \quad (3)$$

As one of the URANS models, the SST model created by Langtry et al. [23] can efficiently combine the k- $\omega$  model in the nearby-wall area and the k- $\epsilon$  model in the far-field to control the complex flows with adverse pressure gradients. Two mathematical expressions, including k and  $\omega$  equations, have been intended in SST approach as below [4]:

$$\begin{aligned} \frac{\partial}{\partial t}(\rho k) + \frac{\partial}{\partial x_i}(\rho k u_i) \\ = \frac{\partial}{\partial x_j} \left( \Gamma_k \frac{\partial k}{\partial x_j} \right) + G_k \\ - Y_k + S_k \end{aligned} \quad (4)$$

$$\begin{aligned} \frac{\partial}{\partial t}(\rho \omega) + \frac{\partial}{\partial x_i}(\rho \omega u_i) \\ = \frac{\partial}{\partial x_j} \left( \Gamma_\omega \frac{\partial \omega}{\partial x_j} \right) + G_\omega \\ - Y_\omega + S_\omega \end{aligned} \quad (5)$$

where  $\Gamma_k$  and  $\Gamma_\omega$  express the active diffusivity of k and  $\omega$ , also  $S_k$  and  $S_\omega$  that are user-defined source terms. Additionally,  $G_k$  and  $G_\omega$  show the turbulence kinetic energy production as a result of mean velocity gradients

and  $\omega$ ,  $Y_k$  and  $Y_\omega$  as well mean the dissipation of  $k$  and  $\omega$  because of turbulence [24].

$$\Gamma_k = \mu + \frac{\mu_t}{\sigma_k} \quad (6)$$

$$\Gamma_\omega = \mu + \frac{\mu_t}{\sigma_\omega} \quad (7)$$

where  $\sigma_k$  and  $\sigma_\omega$  are the turbulent Prandtl numbers for  $k$  and  $\omega$ , respectively. The turbulent viscosity,  $\mu_t$ , is calculated as follows [24]:

$$\mu_t = \frac{\rho k}{\omega} \frac{1}{\max\left[\frac{1}{a^*}, \frac{SF_2}{a_1\omega}\right]} \quad (8)$$

where  $S$  is the strain rate magnitude and

$$\sigma_k = \frac{1}{\frac{F_1}{\sigma_{k,1}} + \frac{(1-F_1)}{\sigma_{k,2}}} \quad (9)$$

$$\sigma_\omega = \frac{1}{\frac{F_1}{\sigma_{\omega,1}} + \frac{(1-F_1)}{\sigma_{\omega,2}}} \quad (10)$$

The most challenging problem utilizing CFD for simulating airflow characteristics around airfoils at low Reynolds number is to catch the stall phenomena. This is a familiar issue and it is mostly as a result of the inadequacy of URANS turbulence models to catch the boundary layer separation caused by the adverse pressure gradient. In particular, at low Reynolds number, an influential part of the boundary layer is laminar so, the use of a typical completely turbulent fails to capture the real boundary layer behavior sufficiently. Actually, the laminar boundary layer is very responsive to adverse pressure gradient and this directs to an earlier separation if evaluated to a turbulent boundary layer and, eventually, in an unrealistic simulation of the initial and deep stall. As the VAWTs work at low Re number, stall phenomena are of vital significance for their modeling. Accordingly, the employment of SST transition model should direct to a more truthful prediction of the airfoils aerodynamic performance [25], and subsequently an improved prediction of the VAWTs performance [20].

The SST transition model is a four-equation turbulence model that merges  $k$ - $\omega$  SST transport equations with two other transport equations, one for intermittency ( $\gamma$ ) and

second for Transition Reynolds number ( $Re_{\theta_t}$ ). Here, intermittency term is used to stimulate the production term of  $k$ , downstream of the transition point in the boundary layer, while the  $Re_{\theta_t}$  term captures the non-local effect of the turbulence intensity. This model is described to have a significant improvement compared with experimental data [23].

Finally, the SST transition model can be written as [26]:

$$\begin{aligned} \frac{\partial}{\partial t}(\rho k) + \frac{\partial}{\partial x_i}(\rho k u_i) &= \frac{\partial}{\partial x_j} \left( \Gamma_k \frac{\partial k}{\partial x_j} \right) + G_k^* \\ &- Y_k^* + S_k \end{aligned} \quad (11)$$

$$\begin{aligned} \frac{\partial}{\partial t}(\rho \omega) + \frac{\partial}{\partial x_i}(\rho \omega u_i) &= \frac{\partial}{\partial x_j} \left( \Gamma_\omega \frac{\partial \omega}{\partial x_j} \right) + G_\omega \\ &- Y_\omega + S_\omega \end{aligned} \quad (12)$$

$$Y_k^* = \min \left( \max(\gamma_{eff}, 0.1) \right) Y_k \quad (13)$$

$$G_k^* = \gamma_{eff} G_k \quad (14)$$

$$\gamma_{eff} = \max(\gamma, \gamma_{sep}) \quad (15)$$

where  $\gamma_{sep}$  is the tailored separation-induced transition.

## 2.2 Key performance parameters

The turbine power output is assessed as the non-dimensional power coefficient  $C_p$  where,

$$C_p = \lambda C_m \quad (16)$$

where the tip speed ratio  $\lambda$  is described as,

$$\lambda = \frac{\omega R}{V} \quad (17)$$

and  $\omega$  is the turbine rotational speed,  $R$  is the turbine radius,  $V$  is the free stream velocity, and the turbine torque  $C_m$  is described as,

$$C_m = \frac{T}{0.5\rho ARV^2} \quad (18)$$

## 2.3 Geometrical models description

In this paper two models were studied to compare different turbulence model. Model (A) was used to validate the present study results with the numerical results obtained by Rezaeiha et al. [16] (Table 1). And model (B) was used to validate the present study results with the numerical and experimental results found by Castelli et al. [22] (Table 2).

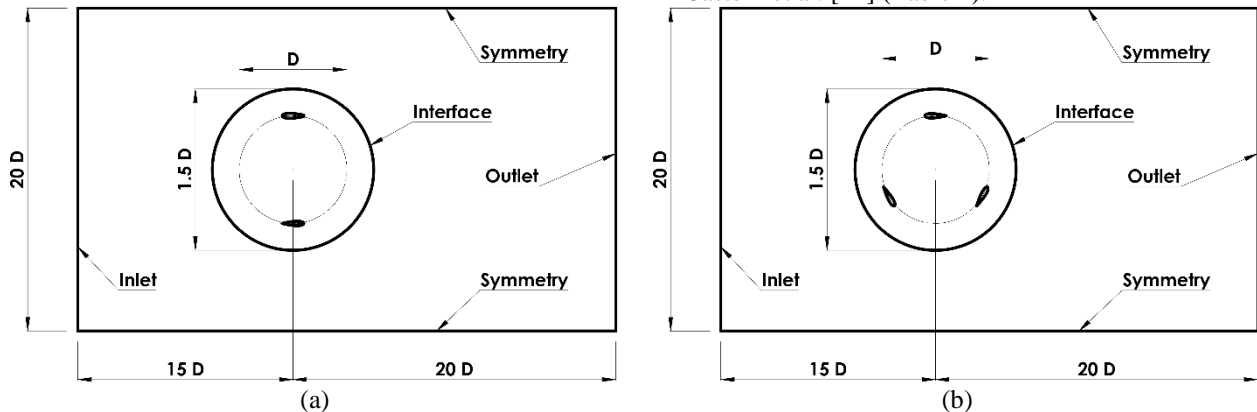


Figure 1: Models Validated through the present study, (a) Model (A) by Rezaeiha (2018), (b) Model (B) by Castelli (2011)

Table 1: Model (A) geometrical and operational parameters

Number of blades	2
Turbine diameter "D" (mm)	1000
Airfoil	NACA 0018
Airfoil chord length (mm)	60
Free stream velocity (m/s)	9.3
Type of generated mesh elements	Triangular
Number of generated mesh elements	196,160

Table 2: Model (B) geometrical and operational parameters

Number of blades	3
Turbine diameter "D" (mm)	1030
Airfoil	NACA 0021
Airfoil chord length (mm)	85.8
Free stream velocity (m/s)	9
Type of generated mesh elements	Triangular
Number of generated mesh elements	231,640

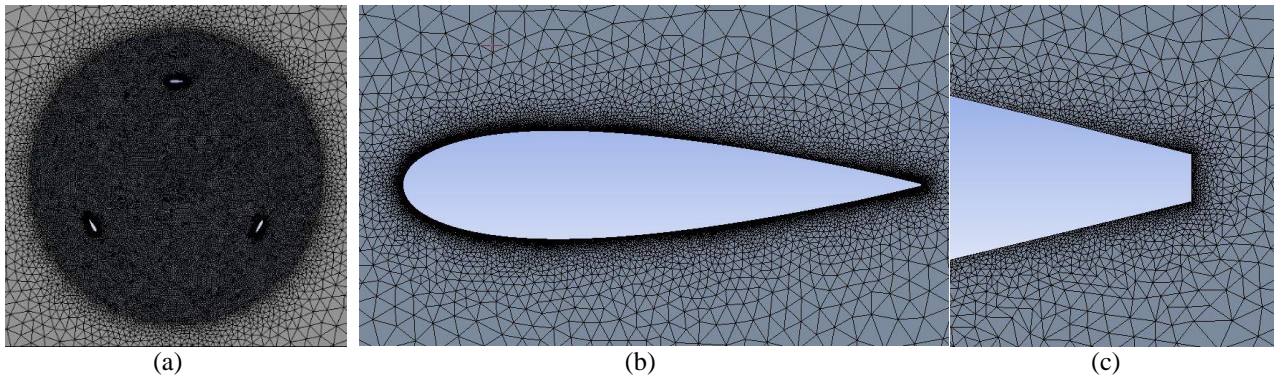


Figure 2: Generated Mesh for Model (B), (a) Turbine Rotor, (b) Airfoil, (c) Trailing Edge

### 3 Results and Discussion

Three different turbulence models were employed with model (A), two equations  $k-\epsilon$  Realizable, two equations  $k-\omega$  SST and four equations Transition-SST, both  $k-\epsilon$  Realizable and Transition-SST showed better results than  $k-\omega$  SST (see Figure 3). However, Transition-SST showed slightly better results than  $k-\epsilon$  Realizable. Accordingly, the  $k-\omega$  SST turbulence model is eliminated in model (B).

On the other hand, two different models were used with model (B), two equations  $k-\epsilon$  Realizable and four equations Transition-SST. The  $k-\epsilon$  Realizable turbulence model has an underestimated power curve compared with the power curve obtained from experimental data. While the Transition-SST turbulence model has an overestimated power curve compared with the power curve obtained from experimental data (see Figure 4).

The observed curves of instantaneous torque coefficient,  $C_m$ , for various turbulence models are attained for model (A) and model (B). As can be observed from the figure, the torque is fluctuating through the revolution of rotor (see Figure 5 & Figure 6). At the beginning revolutions, the oscillation is very strong as the flow has not fully developed. Afterward the curve tends to be more and more systematic and lastly displays cyclic variation. The highest value occurs close to the location where the airfoil chord is perpendicular to the flow

direction in the upwind area and the valleys occur slightly before the location where the airfoil chord is parallel to the flow direction (see Figure 8 & Figure 9).

To realize the differences among the simulation results of the above turbulence models, the details of the flow fields of different turbulence models in a stable period are also investigated. As representatives, the velocity field contours of the flow around blade at different positions (see Figure 7). As can be seen, there is little difference between the velocity magnitudes of the two models around the blade. And the two models can both capture the separation phenomenon of the blade at different positions.

### 4 Conclusion

This study performed CFD simulations employing three different models, the realizable  $k-\epsilon$ , SST  $k-\omega$  and transition SST turbulence models, the outcome of this simulations test pointed out that the realizable  $k-\epsilon$  turbulence model obtained closer results to the experimental data. Precisely, among all turbulence models used in the present study the  $k-\epsilon$  Realizable turbulence model showed the best results. However, the Transition-SST turbulence model showed slightly different results compared with the  $k-\epsilon$  Realizable turbulence model, but better than the results obtained from the  $k-\omega$  SST turbulence model.

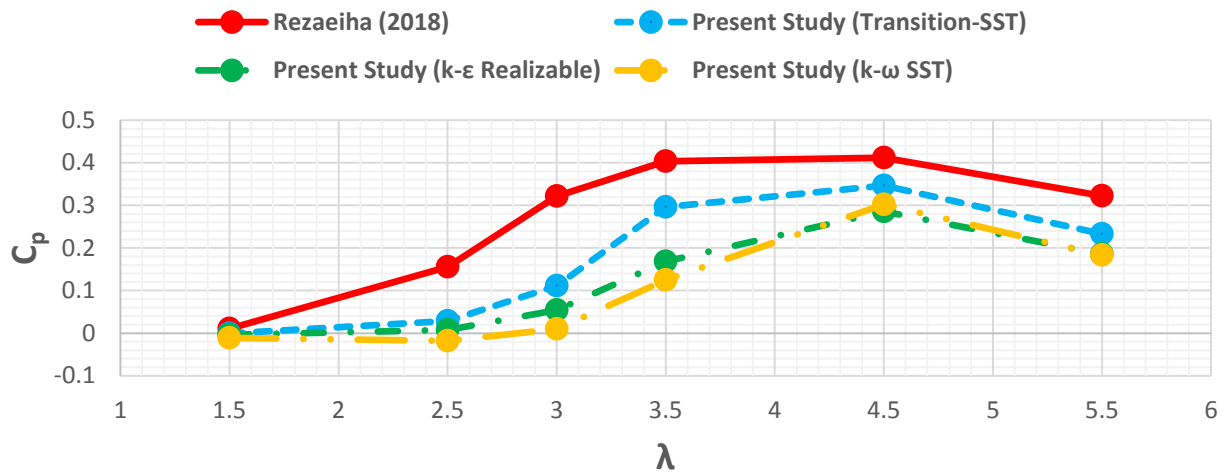


Figure 3: Model (A) power coefficient versus tip speed ratio

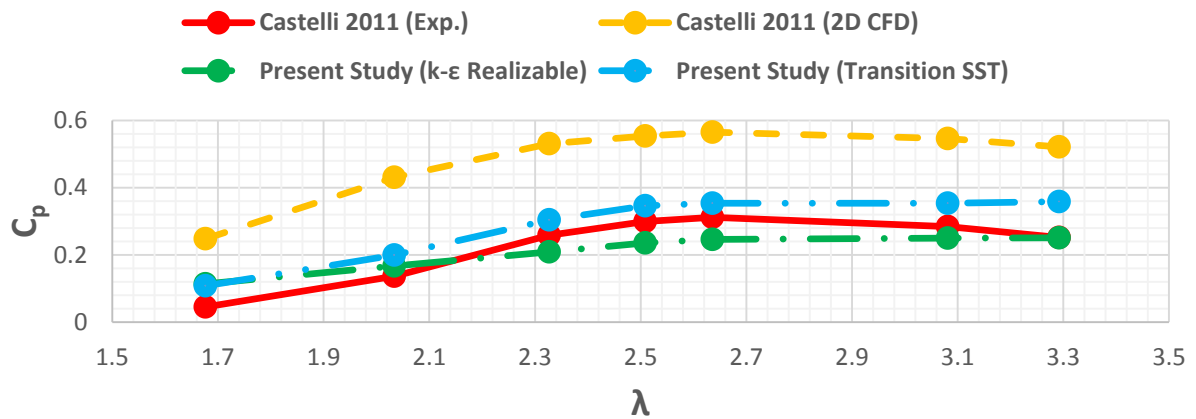


Figure 4: Model (B) power coefficient versus tip speed ratio

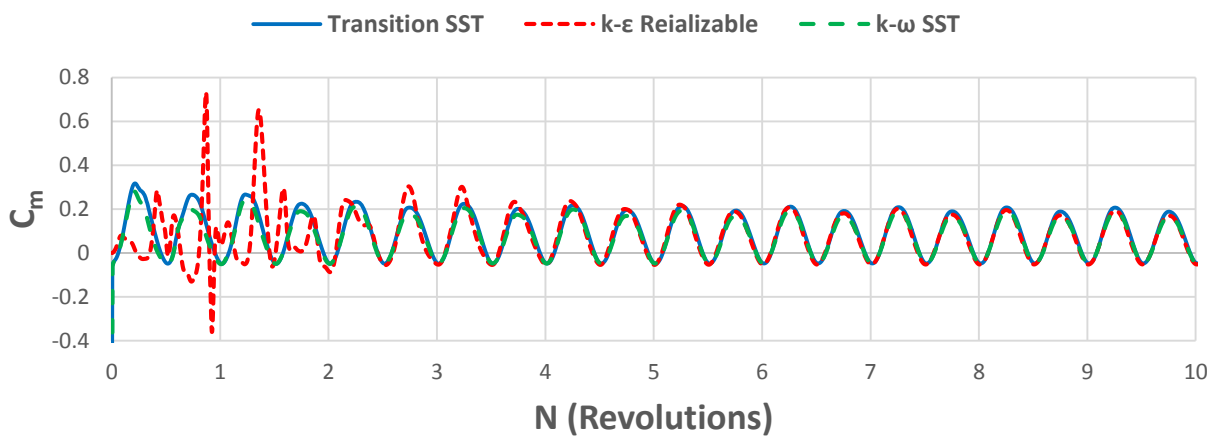


Figure 5: Model (A) instantaneous torque vs number of revolutions

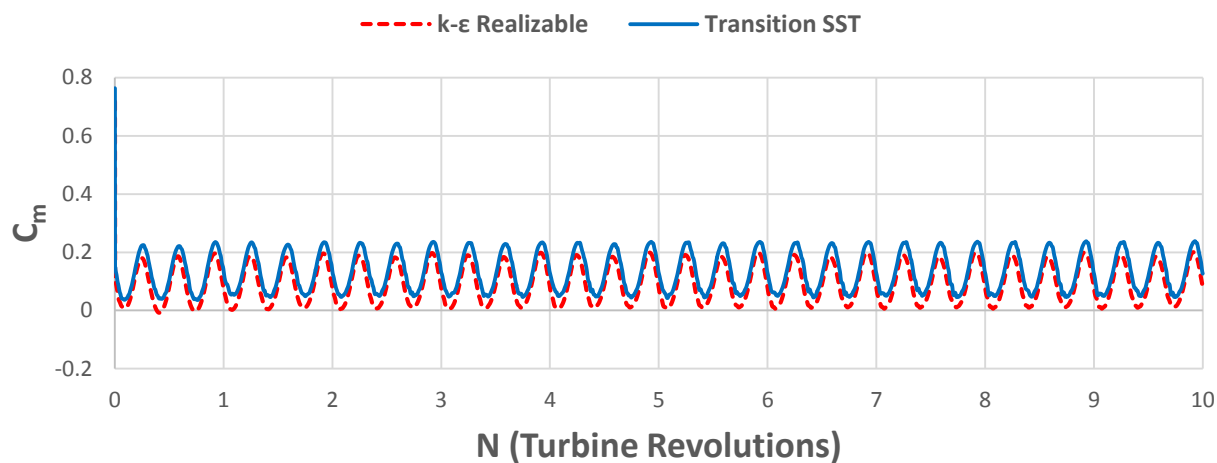
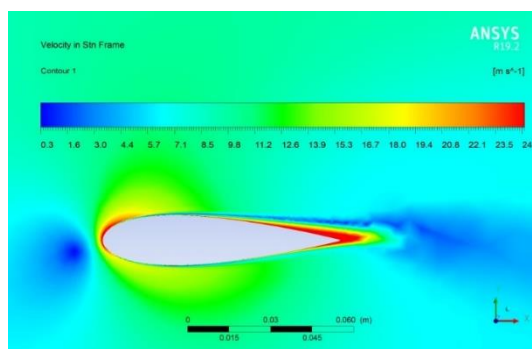


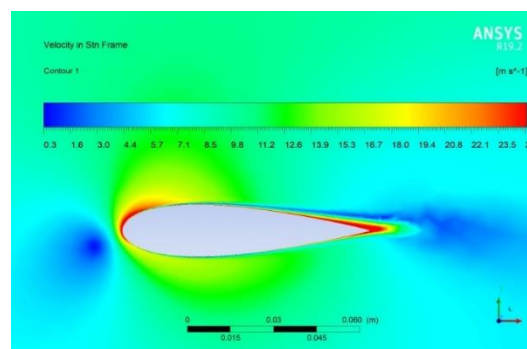
Figure 6: Model (B) instantaneous torque vs number of revolutions

k-ε Realizable Model

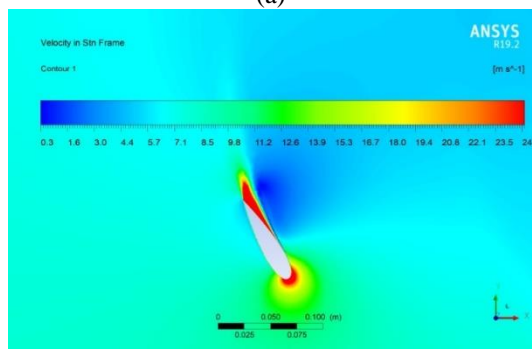
Transition SST Model



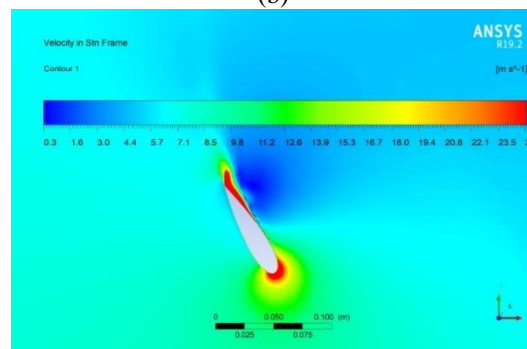
(a)



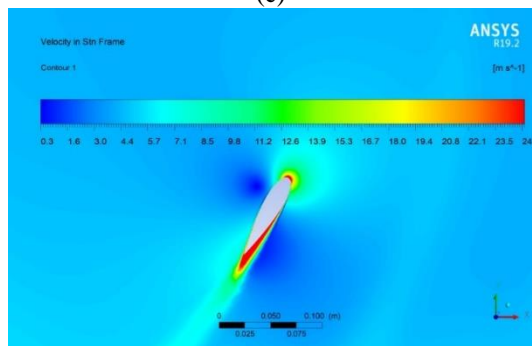
(b)



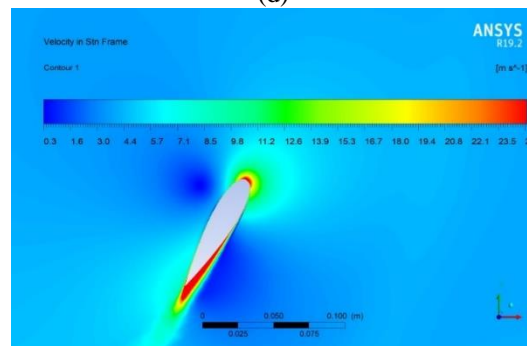
(c)



(d)

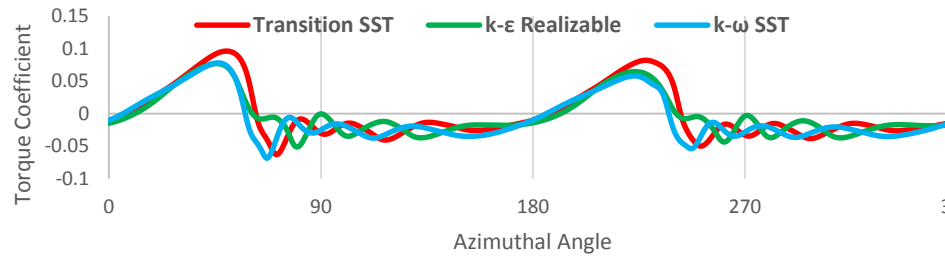


(e)

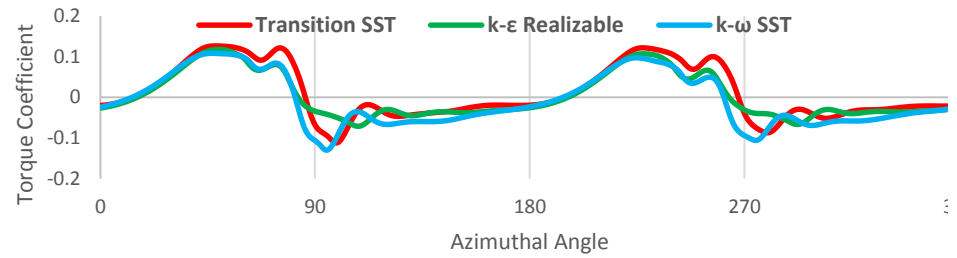


(f)

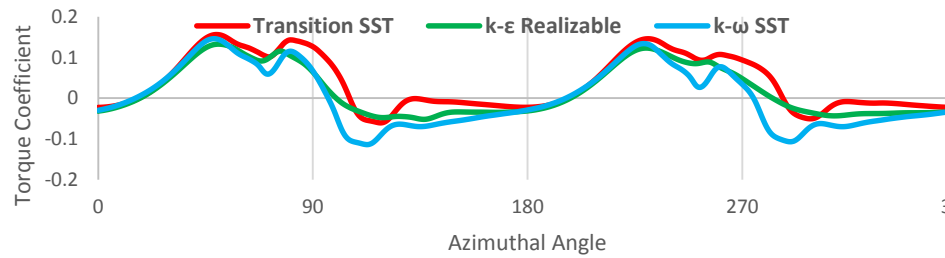
Figure 7: Comparison for the flow fields of the two turbulence models used in model (b) at different positions



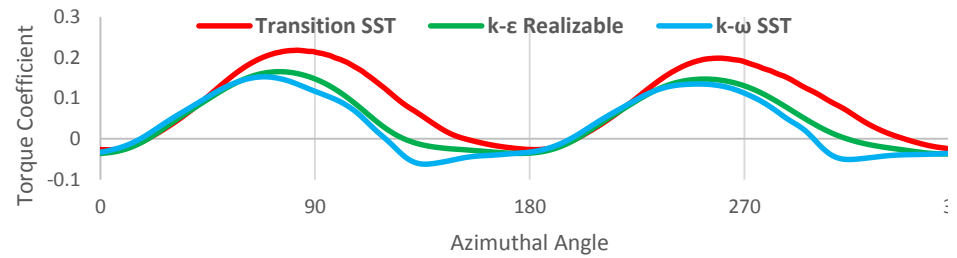
(a)



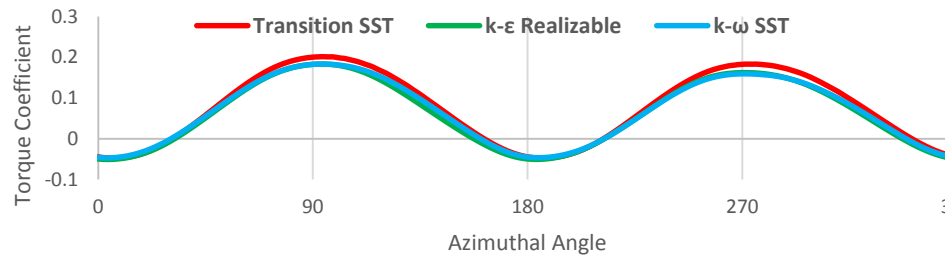
(b)



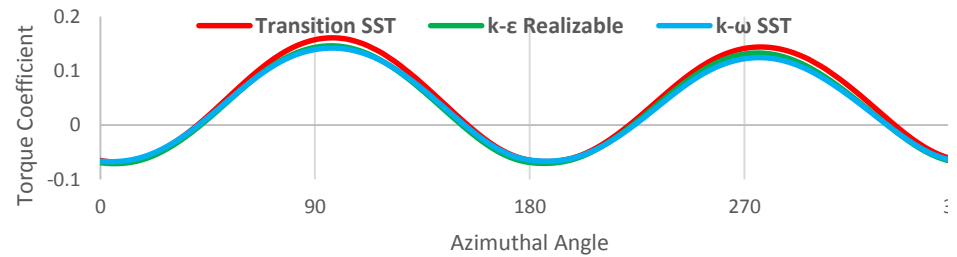
(c)



(d)

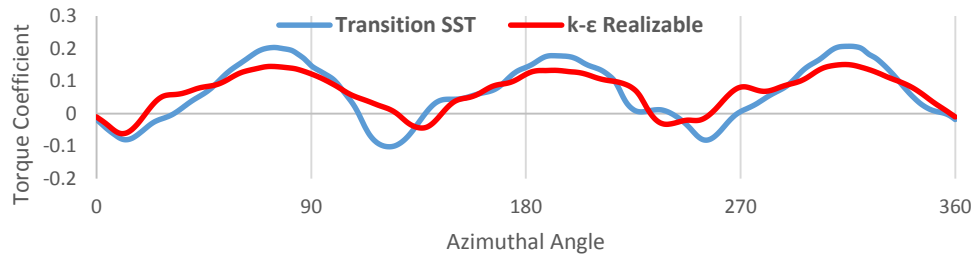


(e)

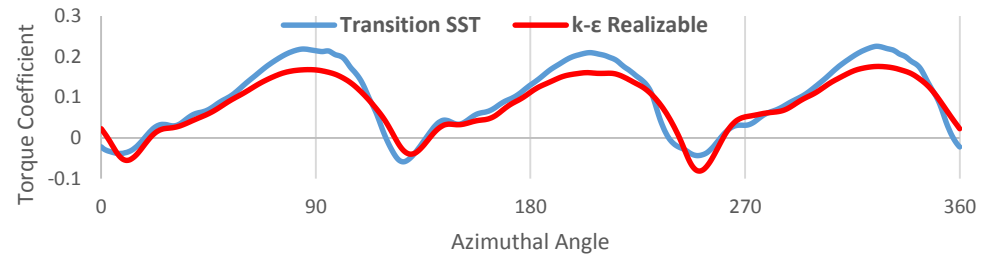


(f)

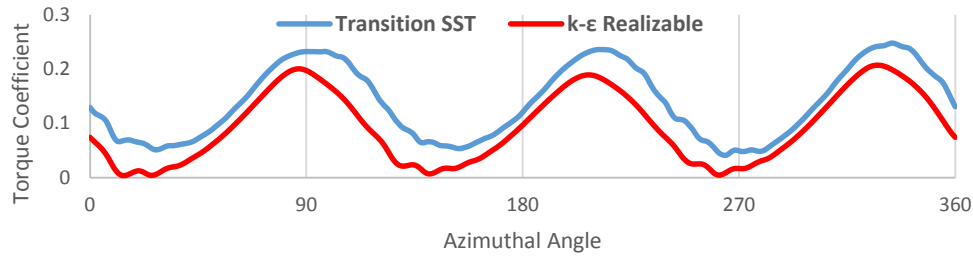
Figure 8: Model (A) last revolution torque coefficient versus azimuthal angle at different tip speed ratios (a)  $\lambda = 1.5$ , (b)  $\lambda = 2.5$ , (c)  $TSR = 3$ , (d)  $\lambda = 3.5$ , (e)  $\lambda = 4.5$ , (f)  $\lambda = 5.5$



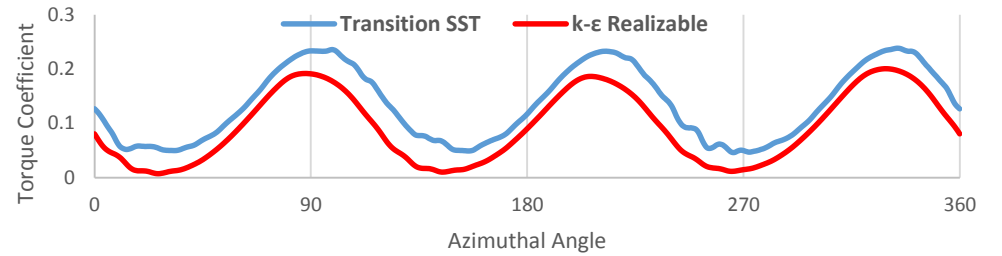
(a)



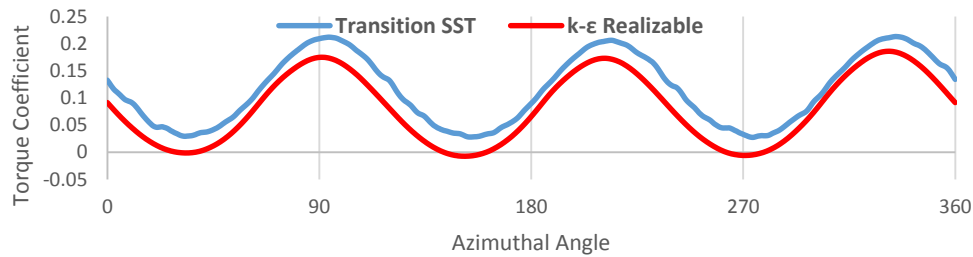
(b)



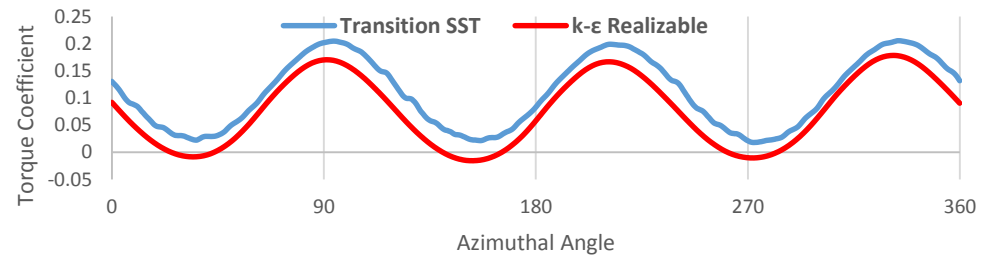
(c)



(d)



(e)



(f)

Figure 9: Model (A) last revolution torque coefficient versus azimuthal angle at different tip speed ratios (a)  $\lambda = 1.7$ , (b)  $\lambda = 2$ , (c)  $\lambda = 2.5$ , (d)  $\lambda = 2.6$ , (e)  $\lambda = 3$ , (f)  $\lambda = 3.3$

## References

- [1] M. Ghasemian, Z. N. Ashrafi, and A. Sedaghat, "A review on computational fluid dynamic simulation techniques for Darrieus vertical axis wind turbines," *Energy Conversion and Management*, vol. 149, pp. 87–100, Oct. 2017.
- [2] J. L. Sawin, K. Seyboth, and F. Sverrisson, *Renewables 2018: Global Status Report*. 2018.
- [3] GWEC, "Global Wind Report - Annual Market Update 2017," 2018.
- [4] Y. Wang, S. Shen, G. Li, D. Huang, and Z. Zheng, "Investigation on aerodynamic performance of vertical axis wind turbine with different series airfoil shapes," *Renewable Energy*, vol. 126, no. 1–4, pp. 801–818, Oct. 2018.
- [5] A. Tummala, R. K. Velamati, D. K. Sinha, V. Indrajaya, and V. H. Krishna, "A review on small scale wind turbines," *Renewable and Sustainable Energy Reviews*, vol. 56, pp. 1351–1371, Apr. 2016.
- [6] W. T. Chong *et al.*, "Cross axis wind turbine: Pushing the limit of wind turbine technology with complementary design," *Applied Energy*, vol. 207, pp. 78–95, Dec. 2017.
- [7] A. Rezaeiha, H. Montazeri, and B. Blocken, "Characterization of aerodynamic performance of vertical axis wind turbines: Impact of operational parameters," *Energy Conversion and Management*, vol. 169, no. May, pp. 45–77, Aug. 2018.
- [8] M. Abkar and J. O. Dabiri, "Self-similarity and flow characteristics of vertical-axis wind turbine wakes: an LES study," *Journal of Turbulence*, vol. 18, no. 4, pp. 373–389, Apr. 2017.
- [9] A. Rezaeiha, I. Kalkman, and B. Blocken, "Effect of pitch angle on power performance and aerodynamics of a vertical axis wind turbine," *Applied Energy*, vol. 197, pp. 132–150, Jul. 2017.
- [10] H.-C. Tsai and T. Colonius, "Coriolis Effect on Dynamic Stall in a Vertical Axis Wind Turbine," *AIAA Journal*, vol. 54, no. 1, pp. 216–226, Jan. 2016.
- [11] A. Rezaeiha, I. Kalkman, H. Montazeri, and B. Blocken, "Effect of the shaft on the aerodynamic performance of urban vertical axis wind turbines," *Energy Conversion and Management*, vol. 149, no. July, pp. 616–630, Oct. 2017.
- [12] E. Möllerström, F. Ottermo, A. Goude, S. Eriksson, J. Hylander, and H. Bernhoff, "Turbulence influence on wind energy extraction for a medium size vertical axis wind turbine," *Wind Energy*, vol. 19, no. 11, pp. 1963–1973, Nov. 2016.
- [13] A. Rezaeiha, H. Montazeri, and B. Blocken, "Towards accurate CFD simulations of vertical axis wind turbines at different tip speed ratios and solidities: Guidelines for azimuthal increment, domain size and convergence," *Energy Conversion and Management*, vol. 156, pp. 301–316, Jan. 2018.
- [14] H. Y. Peng and H. F. Lam, "Turbulence effects on the wake characteristics and aerodynamic performance of a straight-bladed vertical axis wind turbine by wind tunnel tests and large eddy simulations," *Energy*, vol. 109, pp. 557–568, Aug. 2016.
- [15] Z. Wang and M. Zhuang, "Leading-edge serrations for performance improvement on a vertical-axis wind turbine at low tip-speed-ratios," *Applied Energy*, vol. 208, pp. 1184–1197, Dec. 2017.
- [16] A. Rezaeiha, I. Kalkman, and B. Blocken, "CFD simulation of a vertical axis wind turbine operating at a moderate tip speed ratio: Guidelines for minimum domain size and azimuthal increment," *Renewable Energy*, vol. 107, pp. 373–385, Jul. 2017.
- [17] M. H. Mohamed, "Performance investigation of H-rotor Darrieus turbine with new airfoil shapes," *Energy*, vol. 47, no. 1, pp. 522–530, Nov. 2012.
- [18] K. M. Almohammadi, D. B. Ingham, L. Ma, and M. Pourkashan, "Computational fluid dynamics (CFD) mesh independency techniques for a straight blade vertical axis wind turbine," *Energy*, vol. 58, pp. 483–493, Sep. 2013.
- [19] L. Daróczy, G. Janiga, K. Petrasch, M. Webner, and D. Thévenin, "Comparative analysis of turbulence models for the aerodynamic simulation of H-Darrieus rotors," *Energy*, vol. 90, pp. 680–690, Oct. 2015.
- [20] R. Lanzafame, S. Mauro, and M. Messina, "2D CFD Modeling of H-Darrieus Wind Turbines Using a Transition Turbulence Model," *Energy Procedia*, vol. 45, pp. 131–140, 2014.
- [21] R. Gosselin, G. Dumas, and M. Boudreau, "Parametric study of H-Darrieus vertical-axis turbines using CFD simulations," *Journal of Renewable and Sustainable Energy*, vol. 8, no. 5, p. 053301, Sep. 2016.
- [22] M. Raciti Castelli, A. Englaro, and E. Benini, "The Darrieus wind turbine: Proposal for a new performance prediction model based on CFD," *Energy*, vol. 36, no. 8, pp. 4919–4934, 2011.
- [23] R. B. Langtry and F. R. Menter, "Correlation-Based Transition Modeling for Unstructured Parallelized Computational Fluid Dynamics Codes," *AIAA Journal*, vol. 47, no. 12, pp. 2894–2906, Dec. 2009.
- [24] B. Shahizare, N. Nik-Ghazali, W. T. Chong, S. Tabatabaeikia, N. Izadyar, and A. Esmailzadeh, "Novel investigation of the different Omni-direction-guide-vane angles effects on the urban vertical axis wind turbine output power via three-dimensional numerical simulation," *Energy Conversion and Management*, vol. 117, pp. 206–217, Jun. 2016.
- [25] R. Lanzafame, S. Mauro, and M. Messina, "Wind turbine CFD modeling using a correlation-based transitional model," *Renewable Energy*, vol. 52, pp. 31–39, 2013.
- [26] H. Shah, S. Mathew, and C. M. Lim, "Numerical simulation of flow over an airfoil for small wind turbines using the  $\gamma$ -Re $\theta$  model," *International Journal of Energy and Environmental Engineering*, vol. 6, no. 4, pp. 419–429, Dec. 2015.